


# Noninvasive Evaluation of Breast Tumor Response to Combined Ultrasound-Stimulated Microbubbles and Hyperthermia Therapy Using Quantitative Ultrasound-Based Texture Analysis Method

Deepa Sharma, PhD , Lakshmanan Sannachi, PhD, Laurentius Oscar Osapoetra, PhD, Holliday Cartar, BSc, Wentao Cui, BSc, Anoja Giles, BSc, Gregory J. Czarnota, PhD, MD

Received March 6, 2023, from the Physical Sciences, Sunnybrook Research Institute, Toronto, Ontario, Canada (D.S., L.S., L.O.O., H.C., W.C., A.G., G.J.C.); Departments of Medical Biophysics, University of Toronto, Toronto, Ontario, Canada (D.S., L.S., L.O.O., G.J.C.); and Department of Radiation Oncology, Sunnybrook Health Sciences Centre, Toronto, Ontario, Canada (G.J.C.). Manuscript accepted for publication September 23, 2023.

D.S. and L.S. contributed equally to this study.

Address correspondence to Gregory J. Czarnota, PhD, MD, Department of Radiation Oncology, Sunnybrook Health Sciences Centre, 2075 Bayview Avenue, Toronto, Ontario M4N 3M5, Canada. E-mail: [gregory.czarnota@sunnybrook.ca](mailto:gregory.czarnota@sunnybrook.ca)

## Abbreviations

AAC, Average acoustic concentration; ASD, Average scatterer diameter; CON, Contrast; COR, Correlation; ENE, Energy; GLCM, Gray level co-occurrence matrix; H&E, Hematoxylin and eosin; HOM, Homogeneity; ROI, region of interest; HT, Hyperthermia; QUS, Quantitative ultrasound; TUNEL, Terminaldeoxynucleotidyl transferase dUTP nick end labeling; USMB, Ultrasound-stimulated microbubbles

doi:10.1002/jum.16347

This is an open access article under the terms of the [Creative Commons Attribution-NonCommercial-NoDerivs License](https://creativecommons.org/licenses/by-nc/4.0/), which permits use and distribution in any medium, provided the original work is properly cited, the use is non-commercial and no modifications or adaptations are made.

**Objectives**—Quantitative ultrasound (QUS) is a noninvasive imaging technique that can be used for assessing response to anticancer treatment. In the present study, tumor cell death response to the ultrasound-stimulated microbubbles (USMB) and hyperthermia (HT) treatment was monitored *in vivo* using QUS.

**Methods**—Human breast cancer cell lines (MDA-MB-231) were grown in mice and were treated with HT (10, 30, 50, and 60 minutes) alone, or in combination with USMB. Treatment effects were examined using QUS with a center frequency of 25 MHz (bandwidth range: 16 to 32 MHz). Backscattered radiofrequency (RF) data were acquired from tumors subjected to treatment. Ultrasound parameters such as average acoustic concentration (AAC) and average scatterer diameter (ASD), were estimated 24 hours prior and posttreatment. Additionally, texture features: contrast (CON), correlation (COR), energy (ENE), and homogeneity (HOM) were extracted from QUS parametric maps. All estimated parameters were compared with histopathological findings.

**Results**—The findings of our study demonstrated a significant increase in QUS parameters in both treatment conditions: HT alone (starting from 30 minutes of heat exposure) and combined treatment of HT plus USMB finally reaching a maximum at 50 minutes of heat exposure. Increase in AAC for 50 minutes HT alone and USMB +50 minutes was found to be  $5.19 \pm 0.417\%$  and  $5.91 \pm 1.11\%$ , respectively, compared to the control group with AAC value of  $1.00 \pm 0.44\%$ . Furthermore, between the treatment groups,  $\Delta$ ASD-ENE values for USMB +30 minutes HT significantly reduced, depicting  $0.00062 \pm 0.00096\%$  compared to 30 minutes HT only group, showing  $0.0058 \pm 0.0013\%$ . Further, results obtained from the histological analysis indicated greater cell death and reduced nucleus size in both HT alone and HT combined with USMB.

**Conclusion**—The texture-based QUS parameters indicated a correlation with microstructural changes obtained from histological data. This work demonstrated the use of QUS to detect HT treatment effects in breast cancer tumors *in vivo*.

**Key Words**—hyperthermia; quantitative ultrasound; ultrasound-stimulated microbubbles

A deeper understanding of cell death within tumors is vital for the prognosis and prediction of cancer treatment outcomes. Over the past decade, numerous techniques have been developed and are used to determine cellular changes during cancer therapy. Quantitative ultrasound (QUS) is one such modality that is reported to be safe, radiation-free, portable, and cost-effective compared to other commonly used noninvasive imaging techniques.<sup>1,2</sup> Based on the signal intensity, scatter size, and concentration of microscopic scatterers, QUS can easily be employed to differentiate benign versus malignant tumors and healthy functioning cells versus unpaired dead cells.<sup>3-5</sup> Moreover, an easy and rapid way of acquiring and processing data from QUS makes it widely accepted in clinical applications.

The use of QUS for determining tissue structural changes has been implemented clinically as well as in preclinical research. Studies by Czarnota *et al* and Kolios *et al* have discovered earlier that changes in the ultrasound backscatter signal are closely associated with apoptotic cell death. Work by Czarnota and his group indicated a significant increase in ultrasound backscatter signal upon heat treatment in human acute myeloid leukaemia cells (AML-5). The ultrasonic images obtained from both healthy and dead cells exhibited drastic contrast revealing a brighter speckle pattern in apoptotic cells compared to viable cells.<sup>3</sup> Later, Kolios and colleagues demonstrated that several spectral parameters including the mid-band fit (MBF), spectral slope (SS), and 0-MHz intercept (SI) can easily be determined using QUS.<sup>6</sup> Their study showed that these parameters are reflective of nuclear structural changes in tumor cells following treatment. It was confirmed that cells undergoing apoptosis that exhibited features like fragmentation and condensation were primarily responsible for higher MBF and SS. An *in vivo* study suggested a significant elevation in MBF and SS as AML cells underwent the process of apoptosis followed by an exposure to colchicine and DNase, chemical agents known for causing DNA fragmentation and nuclear condensation.<sup>6</sup> Similarly, a preclinical study by Banihashemi *et al* demonstrated mice bearing HTB-67 xenograft when treated with photodynamic therapy resulted in increased MBF and SS displaying greater area of tumor cell death.<sup>7</sup> Many other *in vitro* and *in vivo* studies have confirmed these findings.<sup>8-10</sup>

The use of spectral analysis techniques has also been implemented to differentiate cancer therapy responding patients from nonresponding patients. Patients with breast tumors that responded to chemotherapy exhibited a significant increase in MBF and SS corresponding to greater tumor morphological changes. On the other side, these parameters remain unaltered in nonresponder patients with huge mastectomy malignant masses detected in the histopathological analysis.<sup>5</sup> Other parameters that were found to strongly correlate with tissue morphological changes are average acoustic concentration (AAC) and average scatterer diameter (ASD). A study with breast patients receiving chemotherapy revealed substantial increases in AAC and ASD throughout the treatment duration. No such changes were observed in patients who failed to respond to therapy. Thus, AAC was reported to be the best prognostic marker of treatment response.<sup>11</sup> Similar findings have been validated in the preclinical study suggesting an alteration in AAC and ASD are closely related to tumor cell death and changes in nuclear structures and that these changes are similar to what is seen in its surrogate measures of MBF and SI.

In addition, changes in the gray level co-occurrence matrix (GLCM)-based textural features including contrast (CON), correlation (COR), energy (ENE), and homogeneity (HOM) as a function of the combination of treatments were also investigated. Texture analysis can quantify the heterogeneities of QUS spectral parametric images, providing prognostic factors for cancer characterization.<sup>12-15</sup>

In this study, we aim to extend the understanding and efficacy of QUS-based texture analysis in characterizing tumor structural changes caused by a combination of ultrasound-stimulated microbubbles (USMB) and hyperthermia (HT), a new treatment approach. Here, we investigated the treatment effect (correlation between changes in cell morphology and QUS-based texture measurements) of USMB and HT on breast cancer xenografts (MDA-MB-231) *in vivo*.

## Materials and Methods

### Cell Culture and Animal Model

Human breast cancer MDA-MB-231 cell lines (American Type Culture Collection, ATCC, MD, USA)

were cultured in RPMI—1640 medium supplemented with 10% fetal bovine serum (Sigma Aldrich) and 1% penicillin/streptomycin antibiotic (Thermo Fisher Scientific). Cells were incubated in a 5% CO<sub>2</sub> incubator at 37°C; once the cells reached approximately 80% confluent cells were trypsinized using 0.05% Trypsin-EDTA (Wisent BioProducts). For injection, 5 × 10<sup>6</sup> cells were prepared by resuspending the concentrated cells with 100 μL Mg<sup>+</sup>/Ca + Dulbecco's phosphate buffered saline (DPBS).

For experiments, severe combined immunodeficient (SCID) female mice (Charles River Canada) were used. Tumor cells were injected subcutaneously using a 27 gauge needle in the lower right hind leg of mice. Once the tumor reached the size of 5 to 10 mm in diameter over the 4 to 6 weeks, animals were used for the experiments.

#### **Treatment Overview**

Tumors were exposed to 3% Definity microbubbles, stimulated at 570 kPa ultrasound pressure followed by a 43°C water bath HT treatment for 10, 30, 50, and 60 minutes. Ultrasound backscatter parameters, the AAC and the ASD, and the texture features including CON, COR, ENE, and HOM were estimated from tumors before and 24 hours followed USMB and HT. Changes in these parameters were accounted for monitoring tumor response. Additionally, histological evaluation was performed to complement the results obtained from QUS. A complete detail of USMB and HT treatment is discussed below.

#### **USMB Treatment**

Definity<sup>®</sup> microbubbles (Lantheus Medical Imaging Inc, North Billerica, MA, USA) at a concentration of 3% (v/v), were used for this study. Bubbles were warmed at room temperature before the treatment and were activated by spinning (3000 rpm, 45 seconds) using a Vialmix<sup>®</sup> device (Lantheus Medical Imaging Inc). Microbubble concentration was estimated in accordance with the mean mouse blood volume calculated by the animal's body weight. Microbubbles were diluted in saline (70 μL in 30 μL of heparin saline for 3% doses). Animals to receive USMB therapy were fitted with a tail-vein catheter and secured upright in a water bath at 37°C with the lower body and limbs submerged. The limb bearing the tumor was centered in front of the transducer at a

distance calibrated for maximal focused signal, and immediately before ultrasound exposure, animals were injected with a 100 μL of 3% (v/v) microbubbles in saline followed by 150 μL of 0.2% heparin-saline flush through a tail vein catheter.

The tumors were subsequently and immediately subjected to ultrasound for a treatment duration of 5 minutes using an ultrasound treatment system consisting of a wave-form generator (AWG520, Tektronix), an amplifier (RPR 4000, Ritec), a digital acquisition system (Acqiris DC440/PXI8570, Agilent Technologies Canada, Mississauga, ON, Canada) and a 500 kHz central frequency transducer (Valpey Fisher Inc, MA, USA). Ultrasound parameters used in these experiments were derived from preliminary work<sup>16</sup> and included a 16-cycle tone burst with a 3 kHz pulse repetition frequency resulting in 0.05 seconds in total, followed by no ultrasound for 1.95 seconds to allow the refilling of blood vessels with microbubbles. This resulted in a total pulse sequence of 2 seconds that was continuously repeated for 5 minutes. The transducer was focused at 85 mm and a −6 dB beamwidth of the focal zone was 31 mm. The peak negative pressure was consistent across all treatments at approximately 570 kPa as measured with a calibrated hydrophone, corresponding to a mechanical index of 0.8 at the focus.

#### **HT Treatment**

Tumors were exposed to HT treatment 5 hours after the USMB administration. Treatment was performed using a water bath that maintain water temperature to 43°C. Mice were secured in a ventilated tube in an upright position, allowing the tumor-bearing limb to be submerged in the water bath. In this study, different HT duration was investigated including 10, 30, 50, and 60 minutes.

#### **Histology**

After the 24 hours following treatments, tumors were excised and fixed in 10% neutral buffered formalin (Fisher Scientific Canada, Ottawa, Canada) at room temperature for 48 hours. Tumor sample was then transferred to 70% ethanol. Samples were embedded in paraffin blocks followed by sectioning on glass slides and stained with terminal deoxynucleotidyl transferase dUTP nick end labeling (TUNEL) and hematoxylin and eosin (H&E). TUNEL staining is

used to detect apoptosis and H&E is used to evaluate cell morphology.

Cell death quantification was performed using the images captured at low magnification. Cellular morphology was visualized using both low and high-magnification microscopy (Leica MZ FL III, Leica Microsystems, Concord, ON, Canada).

**Ultrasound Data Acquisition and Analysis**

*Data Collection*

Raw radiofrequency (RF) data were collected 24 hours before and after all treatments using a VisualSonics Vevo770 high-frequency ultrasound imaging system. For this study, an RMV-710B (single-element transducer) operating at 25 MHz center frequency was used. Vevo770 high-frequency ultrasound system has an axial resolution of 54 μm and a lateral resolution of 149 μm. Approximately 60 to 100 RF frames were acquired per scan across the three-dimensional tumor volume.

**QUS Spectral Analysis**

We performed QUS spectral analysis within the two-dimensional regions of interest (ROIs) of the tumor using a sliding window technique. We used a 0.62 mm by 0.62 mm window, with 80% overlap between adjacent windows in both the axial and the lateral directions. The size of the window was carefully selected to encompass an adequate ultrasound wavelengths while preserving the image’s texture. A Hanning window function was used to gate the RF signal along the axial direction for spectral lobes suppression. Spectral contents of the gated RF signal were estimated using the fast Fourier transform (FFT) method over the -6 dB bandwidth of the transducer.<sup>11,17</sup> This corresponds to a range from 10 to 25 MHz. Subsequently, we performed normalization of the power spectrum from the sample to remove instrument-dependent effects, such as transducer focusing. Normalization was performed by dividing the power spectrum from the sample with the power spectrum from a reference phantom, that was scanned using the same ultrasound system and the same acquisition settings. The reference phantom consisted of 5 to 40 μm of glass microspheres embedded in agar gelatin, the attenuation coefficient and speed of sound of the reference phantom were 0.556 dB/MHz/cm and 1540 m/s, respectively.<sup>18</sup> In

order to obtain an accurate power spectrum, point-by-point attenuation compensation was performed to account for the effect of intervening tissue layers.<sup>19</sup> We used attenuation coefficients of α<sub>s</sub> of 2 and 0.6 dB/cm/MHz for the skin and the tumor, respectively, as had been reported in our earlier publication.<sup>18,20,21</sup> The measured backscatter coefficient (σ<sub>Measured</sub>) was obtained from the attenuation-corrected normalized power spectrum,<sup>18</sup> as follows:

$$\sigma_{\text{Measured}}(f) = \frac{S_S(f)}{S_R(f)} e^{4(\alpha_s - \alpha_{\text{Ref}})(R + \frac{\Delta z}{2})} \sigma_{\text{Ref}}(f)$$

where S<sub>S</sub>(f) is the mean power spectrum from the sample, S<sub>R</sub>(f) is the mean power spectrum from the reference phantom, α<sub>s</sub>, and α<sub>Ref</sub> are the attenuation coefficient of the sample, and the reference phantom, respectively, R is the distance from the transducer face to the proximal side of the kernel, Δz is the kernel length, σ<sub>Ref</sub>(f) is the frequency-dependent backscatter coefficient of the reference phantom. Subsequently, we fitted the measured backscatter coefficient (BSC) with the theoretical BSC (σ<sub>Theor</sub>) based on form-factor acoustic scattering models. The theoretical BSC was defined as<sup>19</sup>:

$$\sigma_{\text{Theor}}(f) = \frac{\bar{n}\gamma^2}{9} k^4 a^6 F(k, a)$$

where

$$\gamma^2 \cong 4 \left( \frac{Z_{\text{Scatterer}} - Z_{\text{Background}}}{Z_{\text{Background}}} \right)^2$$

where F(k, a) is the form factor, n̄ denotes the scatterers concentration:= number of scatterers per unit volume, Z is the acoustic impedance, and n̄γ<sup>2</sup> is the AAC, k is the acoustic wave number, and a is the scatterers diameter. AAC and ASD parameters were selected from the theoretical BSC that provides the best fit to the measured BSC.

From the parametric images, mean values and quantitative textural measures were extracted. We used GLCM texture analysis to quantify heterogeneities in the parametric images. The GLCM represents spatial relationships between neighboring pixels in an image (second-order statistics). Symmetric GLCM

matrices were calculated from each parametric image at inter-pixel distances of 1, 2, 3, 4, and 5 (assumed) and four angular directions: 0, 45, 90, and 135. From these GLCM matrices, quantitative textural features that include CON, COR, ENE, and HOM were extracted. These textural measures were subsequently averaged over all GLCM distances and orientations. The textural measures are assumed to be reflected in these averaged values.

### Statistical Analysis

For creating graphs and all the statistical analyses, GraphPad Prism (GraphPad Software, San Diego, CA) and MATLAB 2022 was used. A statistical significance test was performed using the nonparametric Mann-Whitney *U* test. \* $P < .05$  was considered to be statistically significant.

## Results

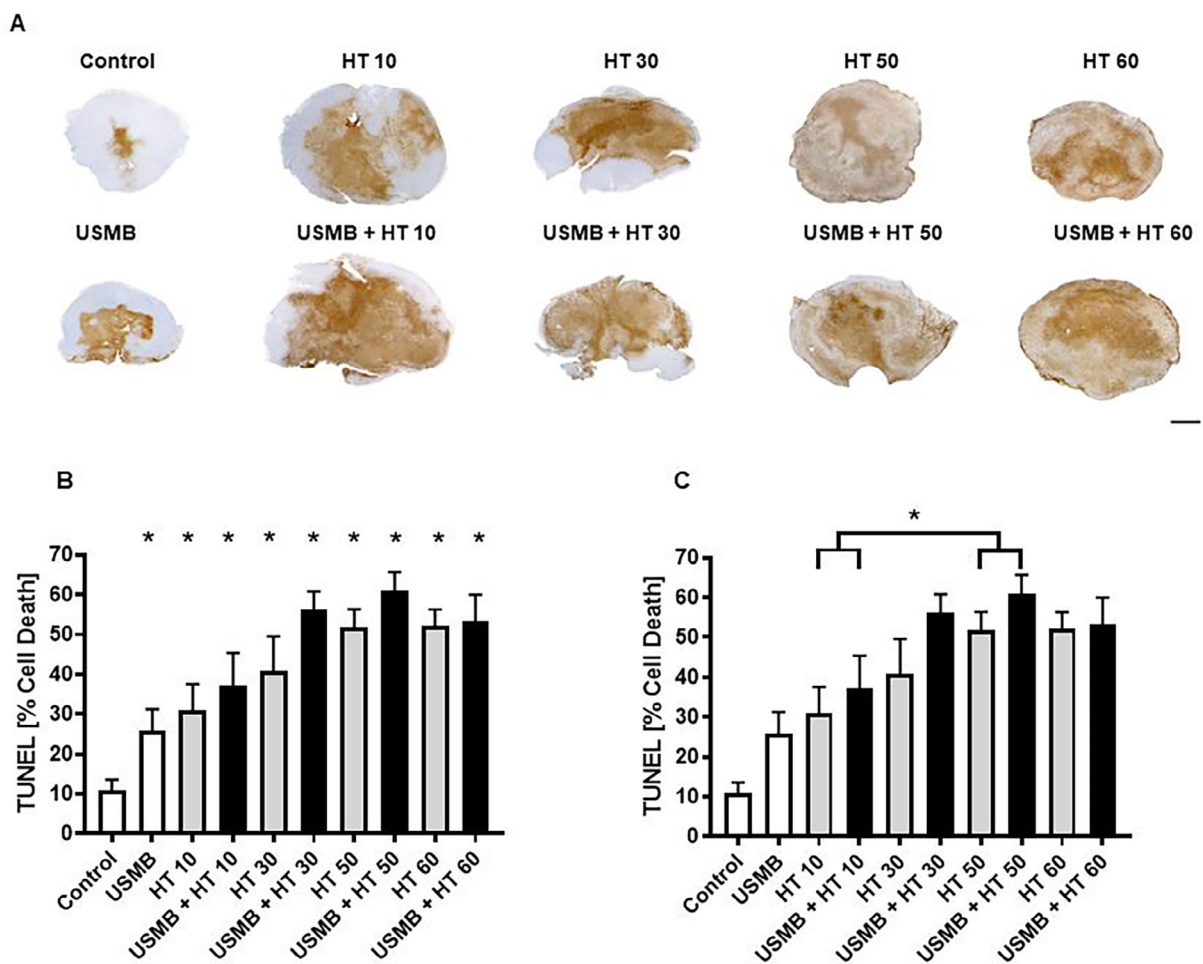
Representative TUNEL histology images from untreated (control), USMB, HT at specific heating times: 10, 30, 50, and 60 minutes, and a combination of USMB + HT at 10, 30, 50, and 60 minutes are displayed in Figure 1A. From these images, we observed significant increases in cell death both in the HT and USMB + HT treatment groups, relative to the control. Figure 1B depicts the quantification of cell death from TUNEL images. The apoptotic cell death percentage was quantified by counting the number of pixels with brown color from TUNEL images. We observed a significant increase in cell death as a function of heating time from both HT and USMB + HT treatment groups, relative to the control. These changes were found to be statistically significant ( $P < .05$ ). Peak cell death was observed in the USMB + HT group at 50 minutes heating. In Figure 1C statistically significant difference in cell death was observed between HT and USMB + HT groups at 50 minutes, compared to that of 10 minutes heating time. This indicates that a combination of treatments is more effective at 50 minutes heating times, as opposed to 10 minutes. Figure 2, A and B presents representative H&E stained images at low and high magnification for control and USMB + HT at 30, 50, and 60 minutes of heating. H&E images from the control show predominantly tumor

cells. On the H&E images from the USMB + HT group, nuclei condensation, and fragmentation were observed. These characterize apoptotic cell death. With USMB + HT 30 minutes, we observed sections that are comprised of tumor cells and condensed nuclei structure. With USMB + HT 50 minutes, we observed sections that show a very dense fragmented nuclei structure. With USMB + HT 60 minutes, nearly half of the cells in the treated area have lost their nuclei as in the final stage of the apoptotic cell death sequence. Figure 2C presents average nucleus sizes measured from different treatment groups using high-magnification images of H&E-stained tumor slices. H&E images were acquired from 5 ROIs and nucleus size was calculated from 40 nuclei from each ROI. A total of 200 nuclei were included from each treatment group to calculate the average nucleus size. Representative posttreatment parametric images of scatterers concentration (AAC) overlaid on B-mode images from control, HT, USMB, and USMB + HT treatment groups are presented in Figure 3. We observed significant increases in the AAC from HT 50 alone and USMB + HT 50 relative to the control. Cell death resulting from a combination of treatments is reflected in the parametric images of AAC. Increasing the treatment effect (heating duration) results in an increase in the changes in AAC. Peak changes in the AAC were observed at 50 minutes heating. A subsequent increase in heating time, for example at 60 minutes heating, results in a decrease in the change in AAC. Figure 4A shows average changes in acoustic concentration for the HT only (gray bars) and for the USMB + HT (dark bars) groups. Significant increases in acoustic concentration were seen in the HT only and the USMB + HT groups ( $P < .05$ ), compared to the control for a heating time of 30 and 50 minutes. At 60 minutes HT, the increase in acoustic concentration diminishes. In Figure 4B we observed statistically significant differences in the changes of acoustic concentration between different USMB + HT treatment groups: 10 and 50 minutes, and 50 and 60 minutes heat exposure times groups. The effect of treatment is more prominent at 50 minutes compared with at 10 minutes, suggesting an optimum time point of 50 minutes as effective HT treatment time. A subsequent increase in treatment does not result in a further increase in AAC. Furthermore, the change in

AAC between 50 and 60 minutes was statistically significant. Figure 5 depicts average changes in AAC-based textural biomarkers of treatment response in the control, HT only, and combined treatment of ultrasound-stimulated vascular disruption and HT for the heating duration of 10, 30, 50, and 60 minutes. The contrast of the AAC map decreases as a function of HT duration from 10 to 50 minutes. On the other hand, the homogeneity of the AAC image shows an increasing trend as a function of HT duration from

10 to 50 minutes. However, these changes were not statistically significant. Changes in textural features were found to be larger for the control and 50-minute heating treatment group and lower for the 30- and 60-minute heating groups. Still, we only observed a statistically significant difference between the control and 60-minute heating treatment group. Figure 6 shows average changes in ASD-ENE, and AAC-COR textural features of treatment response for MDA-MB-231 tumor acquired before treatment, after treatment

**Figure 1.** Representative data obtained from untreated (control), ultrasound-stimulated microbubbles (USMB), hyperthermia (HT), and USMB followed by HT treatment for specific heating time 10, 30, 50, and 60 minutes. **(A)** Low-magnification light microscopy images of TUNEL staining at specific time points after HT treatment. A significant increase in cell death is observed with the HT alone and USMB + HT treatments relative to the control. Scale bar in histology image represent 1 mm. **(B)** Apoptotic cell death percentage (brown area) was quantified from TUNEL image. Increased in cell death with increase in HT time is observed. Error bars represent standard error of the mean and the significant difference between control (untreated animals) versus treated (HT only or USMB + HT treated animals) is indicated by \* for  $P < .05$  using a Mann-Whitney  $U$  test. **(C)** Cell death percentage compared between the heat exposure times from both HT only and combined treatment. Adapted with permission from Sharma et al.<sup>30</sup> Edited by S. H. Dairkee, Figure 4, B and C.



with HT only, and combined USMB and HT for 10, 30, 50, and 60 minutes heat exposure times. We observed significant differences between ASD-ENE, and AAC-COR extracted from 30 minutes HT only and 30 minutes combined USMB and HT heat

exposed groups. GLCM-based texture feature, ENE measures the uniformity in parametric images and correlation measures the correlation between neighbor pixels. Figure 6C depicts low-magnification light microscopy images of TUNEL and H&E staining

**Figure 2.** Representative low (A) and high (B) magnification H&E stained images from control, treated with USMB + HT for 30, 50 and 60 minutes heat exposed sections. Before treatment, whole section were mostly tumor cells. We observed typical changes of apoptosis, including nuclear condensation and fragmentation after treatment. At USMB + 30 minutes heat exposure, sections have mixed normal tumor and condensed nuclei structures. At USMB + 50 minutes heat exposure, sections have mostly very dense fragmented nuclei structure. At USMB + 60 minutes heat exposure, nearly half of the cells in the treated area have lost their nuclei as in a final stage of apoptotic cell death observed clearly at higher magnification (60x). (C) Average nucleus sizes measured for different treatment group using high-magnification images of H&E-stained tumor slices. H&E images were acquired from 5 ROIs and nucleus size were calculated from 40 nucleus from each ROIs. Total of 200 nuclei were included from each treatment group to calculate average nucleus size. Adapted with permission from Sharma *et al.*<sup>31</sup>

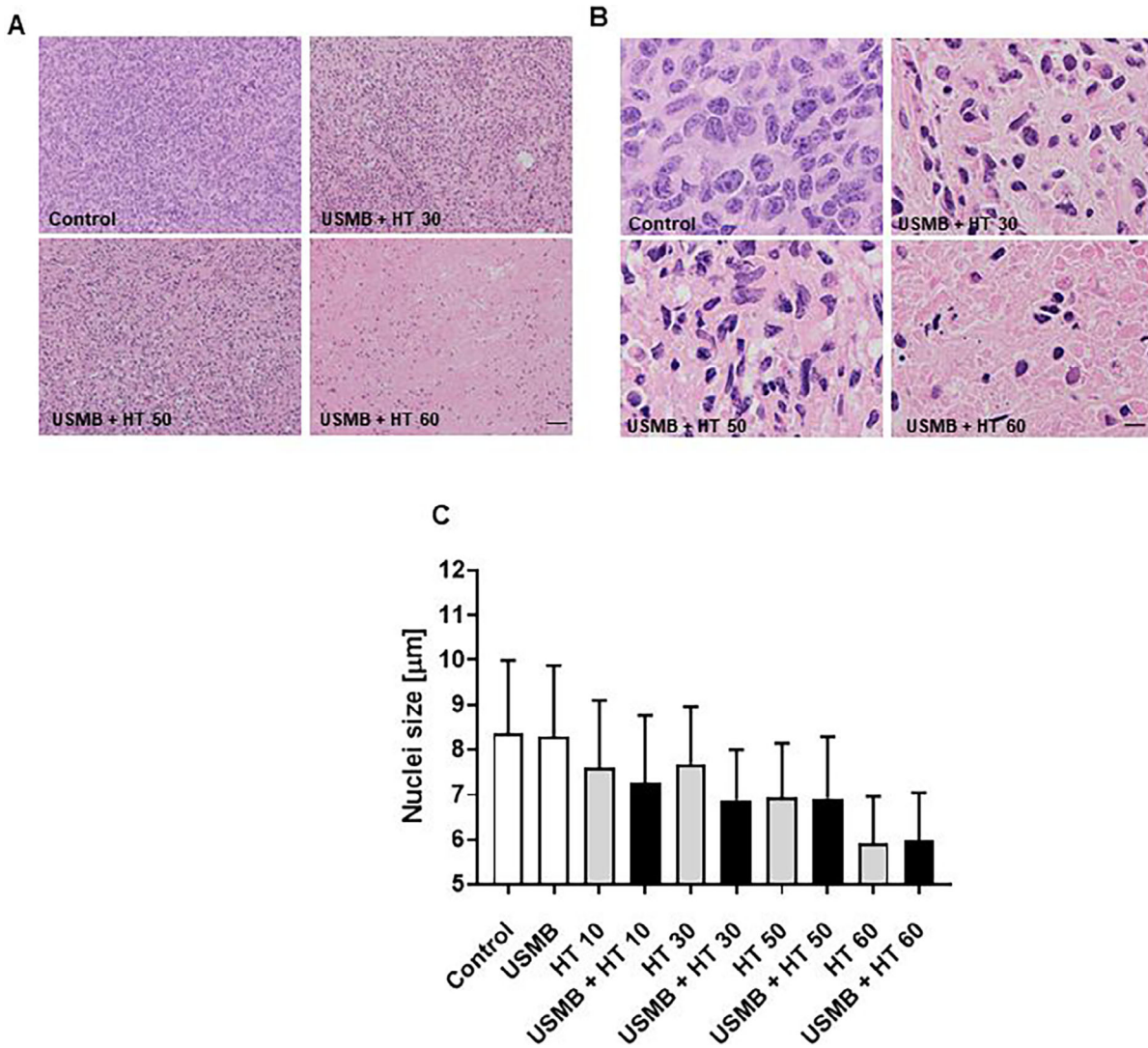


**Figure 3.** High-frequency ultrasound B-mode images with ROI parametric overlays of the average acoustic concentration (AAC) for (A) MDA-MB-231 tumors treated with HT only for 10, 30, 50, and 60 minutes heat and for (B) MDA-MB-231 tumors treated with combined USMB and HT for 10, 30, 50, and 60 minutes. The scale bar in ultrasound images represents 2 mm. The color bar presents range for AAC parameters of 12 to 40 dB/cm<sup>3</sup>.

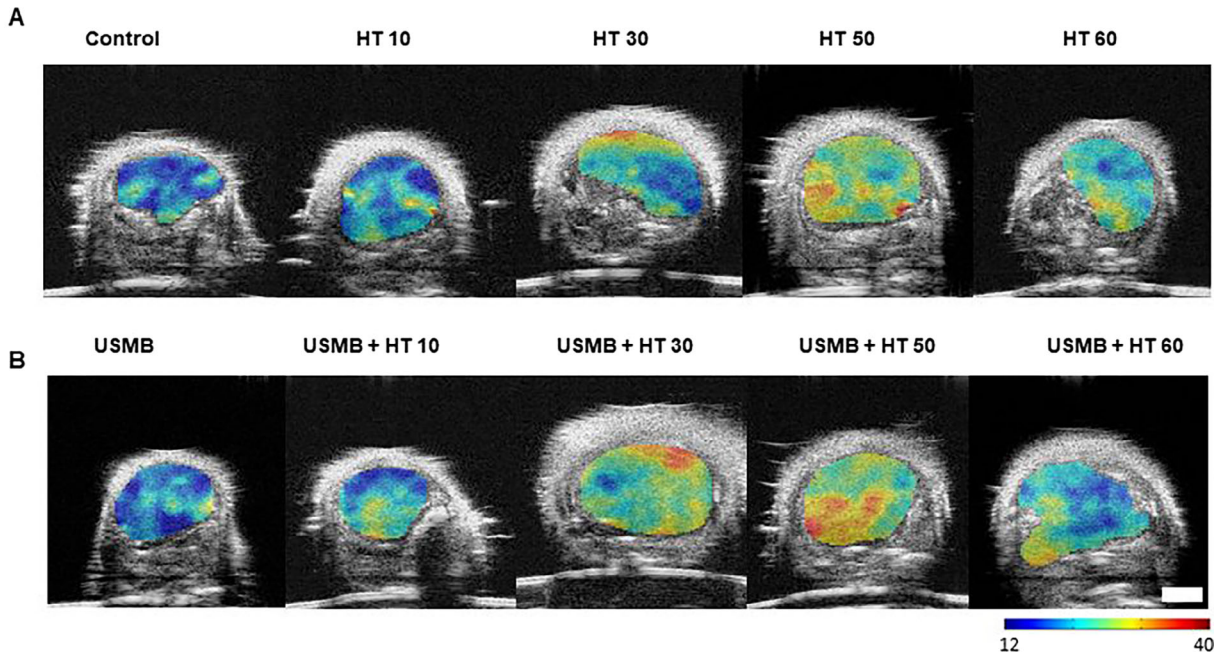
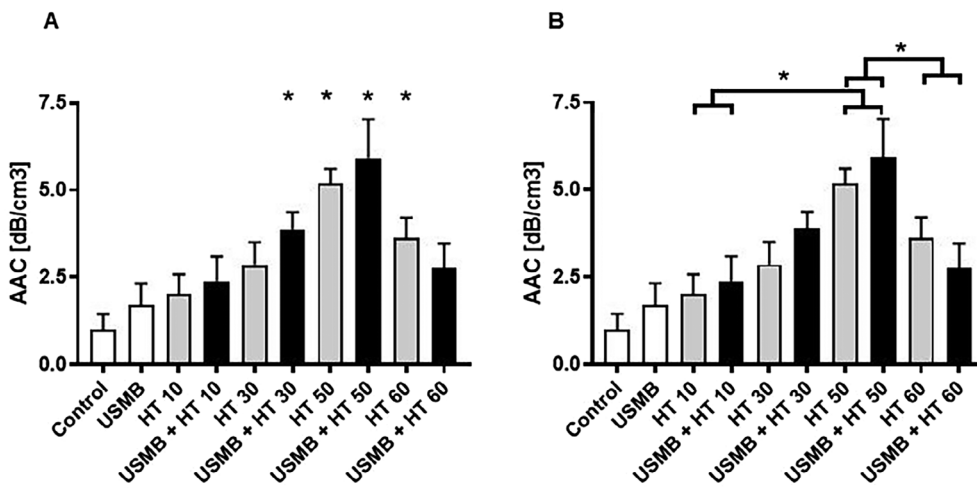


**Figure 4.** Average changes in acoustic concentration in HT only (gray bar) and combined treatment (dark bar) for 10, 30, 50, and 60 minutes heat exposures group of MDA-MB-231 tumors. Control animals are untreated.  $*(P < .05)$  represents the significant difference based on unpaired *t*-test. (A) Comparison of estimated parameters between treated and control group. Significant increase in acoustic concentration was observed from treated group with HT only and combined treatment for heat exposure time 30 and 50 minutes. (B) Comparison between heat exposure times. Significant difference between 10 and 50 minutes, and 50 and 60 minutes heat exposure times groups were observed.





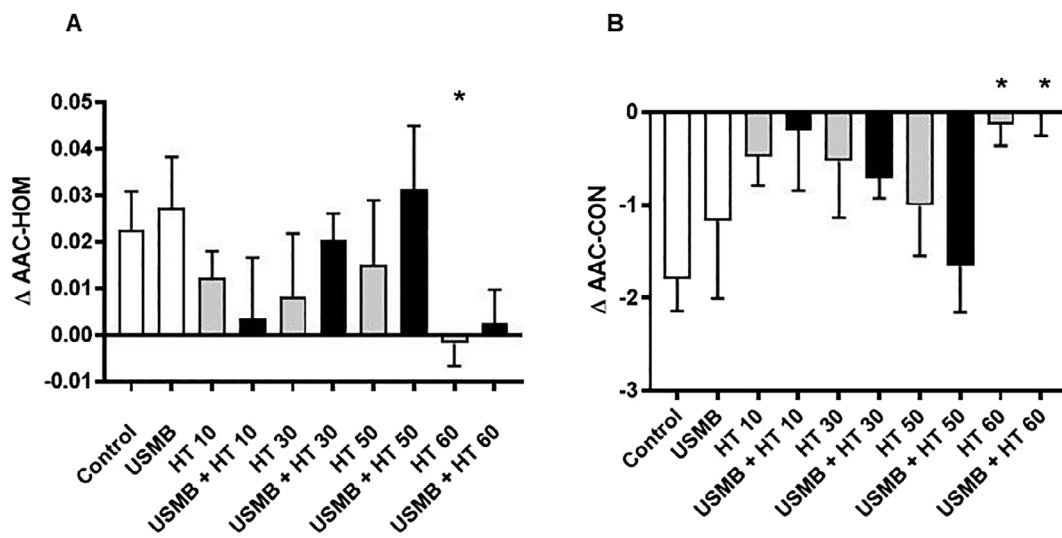
from HT only and combined treatment with 30 minutes heat exposure time. In the HT-treated animal section, the microscopy image demonstrates more cell death close to the skin region and less cell death far from the skin. In the combined treated animal section, the image demonstrates a random amount of cell death in the whole section.

## Discussion

Our previous works have demonstrated a synergistic effect between USMB-induced vascular disruption and radiation therapy (XRT) in killing tumor cells.<sup>16,22,23</sup> In this study, we investigated a combination of cancer therapeutics in USMB-induced vascular disruption and HT (USMB + HT) in an animal model of human breast cancer treatment (MDA-MB-231 cell line). The cancer treatment resulted in cell death as confirmed by histopathological analysis using

TUNEL & H&E histological images. Previous studies conducted with the same treatment modality using the PC3 xenograft model demonstrated greater tumor cell death that was found to be correlated with an increase in QUS backscatter and texture features.<sup>24-26</sup> TUNEL staining revealed a significant increase in cell death from the HT alone and USMB + HT treatment groups relative to the control. In addition, low and high-magnification H&E images also showed areas that demonstrate apoptotic cell death characteristics, including nuclei condensation and fragmentation, especially from the HT alone and USMB + HT groups. Furthermore, we also observed that prolonged heating exposure resulted in an increase in cell death up to a limit, beyond this point further increase in time did not induce a further increase in cell death. The effect of cancer treatment was noninvasively assessed using QUS-based spectroscopy. The increase in cell death as a function of treatment correlates well with changes in the acoustic scattering properties inferred from high ultrasound frequencies. Two

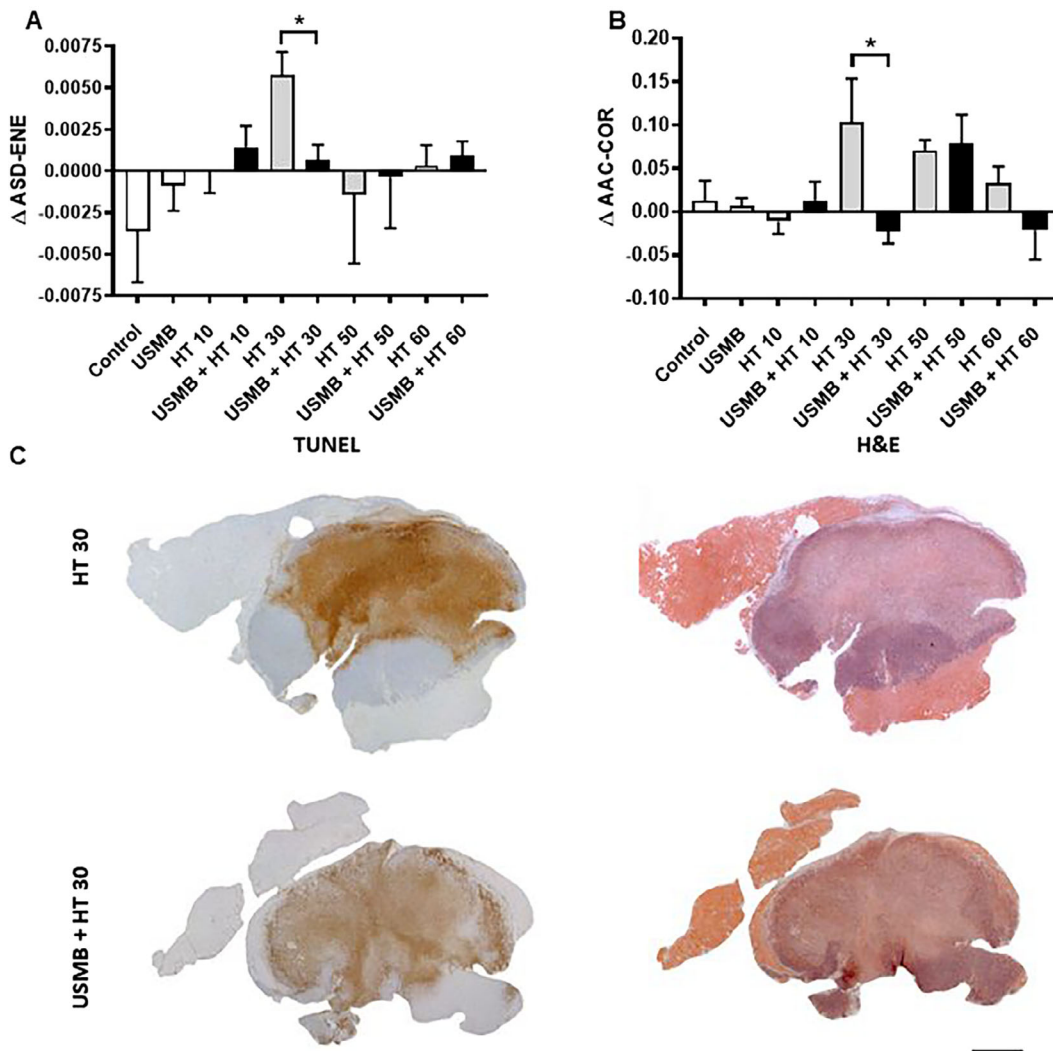
**Figure 5.** Average changes in AAC based-textural biomarkers of treatment response for MDA-MB-231 tumor acquired before treatment, after treatment with HT only, and combined USMB and HT for 10, 30, 50, and 60 minutes heat exposure times (**A** and **B**). Changes in texture features were higher for control and 50 minutes heat exposed groups and smaller for 30 and 60 minutes heat exposed group. However, significant difference were observed only between control and 60 minutes heat exposed groups. Changes in these texture features reflect the changes in microstructure observed in H&E histological sections. For instance, both 30 minutes (normal tumor and condensed nuclei structural regions) and 60 minutes (nuclei fragmented and degenerated regions) heat exposed section have mixed cellular structures. However, control (mostly tumor cell regions) and 50 minutes heat exposed groups (mostly fragmented nuclei structural region) have similar type of structures. These differences in microstructure were reflected in QUS based texture features. Increase in the AAC-HOM detected from control group reflects the increase in number of tumor cells with time (days and weeks) and becoming very dense compact structure.



scattering properties that include AAC and ASD were estimated using the spherical Gaussian model (SGM) to investigate for potential changes in the scatterer's size and scatterer's concentration as tumor cells respond to treatment. Changes in AAC related to cell death were consistent with changes in the surrogate measures of AAC (MBF and SI) and changes in backscatter intensity that had been observed previously both from *in vitro* and from *in vivo* studies but using different treatment modalities.<sup>7,22</sup>

Our working model of ultrasonic scattering properties related to cell death indicates that nuclear changes are predominantly responsible for the increase in AAC. AAC is related to the backscatter amplitude because it is the coefficient of the BSC. The AAC parameter is related to the scatterer's number density and relative acoustic impedance difference between acoustic scatterers and the background. Increases in AAC due to cell death may have been caused by nuclear fragmentation and filling of the

**Figure 6.** Average changes in (A) ASD-ENE, and (B) AAC-COR textural features of treatment response for MDA-MB-231 tumor acquired before treatment, after treatment with HT only, and combined USMB and HT for 10, 30, 50, and 60 minutes heat exposure times. Significant differences were found between ASD-ENE, and AAC-COR extracted from 30 minutes HT only and 30 minutes combined USMB and HT heat exposed groups. (C). Low-magnification light microscopy images of TUNEL and H&E staining from HT only and combined treatment with 30 minutes heat exposure time. The scale bar in histology image represents 1 mm.



extracellular space with cell debris as tumor cells were treated with a combination of treatments of USMB + HT. Previous studies have shown the correlation between changes in the magnitude and the frequency dependence of ultrasonic backscatter and changes in the nuclear structure of the cell.<sup>10</sup>

HT is the use of high temperatures for inducing irreversible cell damage and ultimately tumor apoptosis and coagulative necrosis.<sup>27</sup> In this study, local heating of tumors at 43°C was achieved through external heat application utilizing a water bath. At a temperature range of around 40–45°C, cell damage occurs in an irreversible manner after prolonged heat exposure (ranging from 30 to 60 minutes).<sup>27</sup> This is considered to be the secondary effect of HT. The primary mechanism of HT is inducing direct cell kill by destroying proteins and the structures within cells that occur at temperatures >50°C.<sup>28,29</sup> In the past, HT therapy has been primarily used in conjunction with XRT and chemotherapy for treating cancer.<sup>29</sup> In this work, a novel mode of cancer therapeutic consisting of combined treatment of USMB + HT was investigated. Histopathological analysis confirmed morphological characteristics of both apoptosis and necrosis as a result of the combined treatment. Significant increases in cell death were observed from the TUNEL images of HT alone or USMB + HT treatment groups, relative to the control. At each heating duration, the amount of cell death is higher in the USMB + HT compared to HT groups. Nevertheless, these differences were not statistically significant. In addition, low and high-magnification H&E images from USMB + HT groups also showed nuclei condensation and fragmentation, characteristics of apoptotic cell death. Significant increases in cell death and associated changes in AAC observed beyond 30 minutes USMB + HT groups were consistent with previous works on secondary effects of HT in inducing secondary cell death at prolonged heating exposure.<sup>27</sup> An increase in HT duration resulted in a greater effect on tumor cells killing. Peak cell death was observed at 50 minutes heating in the USMB + HT group. A subsequent increase in the heating duration resulted in a decrease in cell death. This observation can be attributed to the fact that at 60 minutes heating, nearly half of the cells in the treated area have lost their nuclei as in the final stage of apoptosis, as shown from the H&E images. The

plateauing of the average cell death as a function of treatment (HT duration) correlated well with the plateauing observed in the average AAC. This effect is shown in Figure 4B, where a maximum change in the average AAC was observed at 50 minutes heat exposure in the USMB + HT group. An increase in cell death from histology increased the acoustic backscattering as inferred from the AAC parameter. The plateauing of the AAC beyond 50 minutes HT duration resulted from a decrease in acoustic backscattering as nearly half of the cells in the treated area have lost their nuclei.

USMB + HT cancer treatment resulted in morphological characteristics of apoptosis and necrosis. Cell death resulted in a decrease in average cell size. A decrease in average cell size from the HT alone or USMB + HT treatment groups indicates the presence of tumor cells with a smaller size than those of the untreated control group. This is consistent with tumor cells that undergo apoptotic sequence, where they exhibit characteristic features of apoptosis that include shrinkage and convolution. These imply a decrease in average cell size as measured from histology. The minimum average nucleus size was seen in the USMB + HT at 60 minutes heating. Although a decrease in cell size was observed (relative to the control), there was no statistically significant difference between groups at different heating times.

A decrease in cell size observed from histology could not be well characterized by scatterer diameter estimates using SGM. This can be attributed to the fact that ASD estimates using SGM model was considerably larger than the cells (two times larger). We hypothesize that acoustic scattering arises from clusters of predominantly tumor cells, along with a contribution from microvessels, and not from individual cells. At 25 MHz frequency, the backscatter RF signal from the tumor is characterized by Rayleigh and Mie scattering.<sup>10</sup> Rayleigh scattering predominates in the region of very small particles compared to the acoustic wavelength. This includes DNA fragments from cell death. On the other hand, Mie scattering predominates in the region of scattering structures comparable to the acoustic wavelength. Clusters of apoptotic cells, nuclear coalescence, and condensation in the proximity of dying tumor cells may have been contributing to the Mie scattering. These biological features of cell death may have contributed to the

increase in acoustic backscattering as quantified through the AAC parameter. According to the theoretical framework of ultrasonic spectrum analysis developed by Lizzi *et al*,<sup>29</sup> an increase in the scatterers' diameters may also cause an increase in the spectral intercept from the linear regression analysis. Although we observed a decrease in the nuclear size as quantified from histology, mechanical characteristics such as particle density and concentration of scatterers may have contributed to the increase in AAC. An increase in AAC can be attributed to nuclear-scattering changes following cell death.

Heterogeneity in tumor microenvironment, physiology, and metabolism has demonstrated diagnostic and prognostic values in cancer characterization. In this study, we quantify the heterogeneity of the parametric images of QUS imaging biomarkers using the GLCM method. Changes in the average texture measures of QUS spectral maps presented a less clear pattern in indicating therapy effect. The only statistically significant difference between changes in the texture features of the spectral maps was observed only in treatment groups with 60 minutes heating. The animals in the control group did not receive any treatment. The change in the AAC map in the control group can be attributed to the inherent spatial heterogeneities of the tumor. We obtained an average AAC value from 10 representative AAC slices at pretreatment and posttreatment, respectively. However, pretreatment and posttreatment slices are not aligned. Precise alignment would incur more technical experimental difficulties in identifying and utilizing some sorts of markers for exact alignment. Ideally, exact slices from pre- and posttreatment should be compared. In such a setting, the change in AAC should be negligible for the control group. Nevertheless, even with the presence of this limitation to our study, changes in acoustic backscattering resulting from cell death are still able to be detected from QUS analysis. Tumor microstructures alterations is the dominant component to the change in AAC. The statistical analysis suggests that changes in the AAC from the specific treatment groups are statistically significantly higher than that in the control group, allowing a change in AAC to be utilized as an effective imaging biomarker for assessing therapy response.

An increase in the AAC-HOM detected from the control reflects the increase in the number of

tumor cells with time (days and weeks) and becomes a very dense compact structure. Homogeneity quantifies the incidence of pixels with the same intensities. As the tumor microenvironment becomes more regular with fragmented nuclei and cell debris in the extracellular matrix, the homogeneity of AAC parametric images increases. Although these trends are present, a statistically significant difference was observed only in the 60 minutes HT (for AAC-HOM) and 60 minutes HT and USMB + HT (for AAC-CON). Significant differences were also found between ASD-ENE, and AAC-COR extracted from 30 minutes HT only and 30 minutes combined USMB + HT groups. GLCM-based texture feature, energy (ENE) measures the uniformity in parametric images, and correlation measures the correlation between neighbor pixels. More cell death was observed close to skin region in HT 30 animal section (Figure 6C). This suggests that 30 minutes of exposure time is not sufficient to reach our target temperature in the whole tumor. This gradual difference in the amount of cell death observed within the tumor region close to or far from the skin region was reflected in some of the texture features extracted from ultrasound data including ASD-ENE and AAC-COR (Figure 6A and B).

A limitation of this study is that the sequencing effect of the components of combined cancer therapeutics was not investigated. In this study, the therapy sequence consists of the introduction of microbubbles followed by ultrasound exposure. Subsequently, HT was administered for a specific heating duration.

## Conclusion

The present study uses HT as the primary cancer treatment, in conjunction with USMB-induced vascular disruption to treat breast tumor xenograft. In conclusion, we obtained further evidence of the usefulness of QUS-based biomarkers to noninvasively assess the efficacy of anticancer treatment. Change in the size of the cell nucleus associated with cell death post-USMB and HT was correlated with changes in QUS texture features. In particular, the AAC showed a good correlation with tumor cell death.

## Data Availability Statement

The data that supports the findings are available on request from the corresponding author [GJC].

## References

- Deshpande N, Needles A, Willmann JK. Molecular ultrasound imaging: current status and future directions. *Clin Radiol* 2010; 65: 567–581. <https://doi.org/10.1016/j.crad.2010.02.013>.
- Wells PNT, Liang HD. Medical ultrasound: imaging of soft tissue strain and elasticity. *J R Soc Interface* 2011; 8:1521–1549. <https://doi.org/10.1098/rsif.2011.0054>.
- Czarnota GJ, Kolios MC, Vaziri H, et al. Ultrasonic bio-microscopy of viable, dead and apoptotic cells. *Ultrasound Med Biol* 1997; 23:961–965. [https://doi.org/10.1016/S0301-5629\(97\)00067-7](https://doi.org/10.1016/S0301-5629(97)00067-7).
- Vlad RM, Alajez NM, Giles A, Kolios MC, Czarnota GJ. Quantitative ultrasound characterization of cancer radiotherapy effects in vitro. *Int J Radiat Oncol Biol Phys* 2008; 72:1236–1243. <https://doi.org/10.1016/j.ijrobp.2008.07.027>.
- Sadeghi-Naini A, Papanicolau N, Falou O, et al. Quantitative ultrasound evaluation of tumor cell death response in locally advanced breast cancer patients receiving chemotherapy. *Clin Cancer Res* 2013; 19:2163–2174. <https://doi.org/10.1158/1078-0432.CCR-12-2965>.
- Kolios MC, Czarnota GJ, Lee M, Hunt JW, Sherar MD. Ultrasonic spectral parameter characterization of apoptosis. *Ultrasound Med Biol* 2002; 28:589–597. [https://doi.org/10.1016/S0301-5629\(02\)00492-1](https://doi.org/10.1016/S0301-5629(02)00492-1).
- Banihashemi B, Vlad R, Debeljevic B, Giles A, Kolios MC, Czarnota GJ. Ultrasound imaging of apoptosis in tumor response: novel preclinical monitoring of photodynamic therapy effects. *Cancer Res* 2008; 68:8590–8596. <https://doi.org/10.1158/0008-5472.CAN-08-0006>.
- Kim HC, Al-Mahrouki A, Gorjizadeh A, Sadeghi-Naini A, Karshafian R, Czarnota GJ. Quantitative ultrasound characterization of tumor cell death: ultrasound-stimulated microbubbles for radiation enhancement. *PLoS One* 2014; 9:e102343. <https://doi.org/10.1371/journal.pone.0102343>.
- Pasternak MM, Wirtzfeld LA, Kolios MC, Czarnota GJ. High-frequency ultrasound analysis of post-mitotic arrest cell death. *Oncoscience* 2016; 3:109–121. <https://doi.org/10.18632/oncoscience.301>.
- Tran WT, Sannachi L, Papanicolau N, et al. Quantitative ultrasound imaging of therapy response in bladder cancer in vivo. *Oncoscience* 2016; 3:122–133. <https://doi.org/10.18632/oncoscience.302>.
- Sannachi L, Tadayyon H, Sadeghi-Naini A, et al. Non-invasive evaluation of breast cancer response to chemotherapy using quantitative ultrasonic backscatter parameters. *Med Image Anal* 2015; 20:224–236. <https://doi.org/10.1016/j.media.2014.11.009>.
- Sadeghi-Naini A, Suraweera H, Tran WT, et al. Breast-lesion characterization using textural features of quantitative ultrasound parametric maps. *Sci Rep* 2017; 7:13638. <https://doi.org/10.1038/s41598-017-13977-x>.
- Sadeghi-Naini A, Sannachi L, Tadayyon H, et al. Chemotherapy-response monitoring of breast cancer patients using quantitative ultrasound-based intra-tumour heterogeneities. *Sci Rep* 2017; 7: 10352. <https://doi.org/10.1038/s41598-017-09678-0>.
- Osapoetra LO, Sannachi L, DiCenzo D, Quiaoit K, Fatima K, Czarnota GJ. Breast lesion characterization using quantitative ultrasound (QUS) and derivative texture methods. *Transl Oncol* 2020; 13:100827. <https://doi.org/10.1016/j.tranon.2020.100827>.
- Osapoetra LO, Chan W, Tran W, Kolios MC, Czarnota GJ. Comparison of methods for texture analysis of QUS parametric images in the characterization of breast lesions. *PLoS One* 2020; 15: e0244965. <https://doi.org/10.1371/journal.pone.0244965>.
- Czarnota GJ, Karshafian R, Burns PN, et al. Tumor radiation response enhancement by acoustical stimulation of the vasculature. *Proc Natl Acad Sci U S A* 2012; 109:E2033–E2041. <https://doi.org/10.1073/pnas.1200053109>.
- Oelze ML, O'Brien WD. Improved scatterer property estimates from ultrasound backscatter for small gate lengths using a gate-edge correction factor. *J Acoust Soc Am* 2004; 116:3212–3223. <https://doi.org/10.1121/1.1798353>.
- Yao LX, Zagzebski JA, Madsen EL. Backscatter coefficient measurements using a reference phantom to extract depth-dependent instrumentation factors. *Ultrasound Imaging* 1990; 12:58–70. <https://doi.org/10.1177/016173469001200105>.
- Wagner RF, Brown DG, Hall TJ. Describing small-scale structure in random media using pulse-echo ultrasound. *J Acoust Soc Am* 1990; 87:179–192. <https://doi.org/10.1121/1.399283>.
- Vlad RM, Brand S, Giles A, Kolios MC, Czarnota GJ. Quantitative ultrasound characterization of responses to radiotherapy in cancer mouse models. *Clin Cancer Res* 2009; 15:2067–2075. <https://doi.org/10.1158/1078-0432.CCR-08-1970>.
- Vlad RM, Kolios MC, Moseley JL, Czarnota GJ, Brock KK. Evaluating the extent of cell death in 3D high frequency ultrasound by registration with whole-mount tumor histopathology. *Med Phys* 2010; 37:4288–4297. <https://doi.org/10.1118/1.3459020>.
- Lee J, Karshafian R, Papanicolau N, Giles A, Kolios MC, Czarnota GJ. Quantitative ultrasound for the monitoring of novel microbubble and ultrasound radiosensitization. *Ultrasound Med Biol* 2012; 38:1212–1221. <https://doi.org/10.1016/j.ultrasmedbio.2012.01.028>.
- El Kaffas A, Gangeh MJ, Farhat G, et al. Tumour vascular shutdown and cell death following ultrasound-microbubble enhanced radiation

- therapy. *Theranostics* 2018; 8:314–327. <https://doi.org/10.7150/thno.19010>.
24. Sharma D, Giles A, Hashim A, et al. Ultrasound microbubble potentiated enhancement of hyperthermia-effect in tumours. *PLoS One* 2019; 14:e0226475. <https://doi.org/10.1371/journal.pone.0226475>.
  25. Sharma D, Osapoetra LO, Faltyn M, et al. Quantitative ultrasound characterization of therapy response in prostate cancer in vivo. *Am J Transl Res* 2021; 13:4437–4449.
  26. Sharma D, Osapoetra LO, Faltyn M, Giles A, Stanisz M, Czarnota GJ. In vivo assessment of prostate cancer response using quantitative ultrasound characterization of ultrasonic scattering properties. *BMC Cancer* 2021; 21:991. <https://doi.org/10.1186/s12885-021-08706-7>.
  27. Chu KF, Dupuy DE. Thermal ablation of tumours: biological mechanisms and advances in therapy. *Nat Rev Cancer* 2014; 14: 199–208. <https://doi.org/10.1038/nrc3672>.
  28. Jha S, Sharma PK, Malviya R. Hyperthermia: role and risk factor for cancer treatment. *Achiev Life Sci* 2016; 10:161–167. <https://doi.org/10.1016/j.als.2016.11.004>.
  29. Coleman J, Greenebaum M, Feleppa EJ, Elbaum M. Theoretical framework for spectrum analysis in ultrasonic tissue characterization. *J Acoust Soc Am* 1983; 73:1366–1373. <https://doi.org/10.1121/1.389241>.
  30. Sharma D, Cartar H, Law N, et al. Optimization of microbubble enhancement of hyperthermia for cancer therapy in an in vivo breast tumour model. *PLoS One* 2020; 15:e0237372. <https://doi.org/10.1371/journal.pone.0237372>.
  31. Sharma D, Carter H, Sannachi L, et al. Quantitative ultrasound for evaluation of tumour response to ultrasound-microbubbles and hyperthermia. *Technol Cancer Res Treat* 2023. <https://doi.org/10.1177/15330338231200993>.